A simplified approach for heat conduction analysis of CNT-based nano-composites

Jianming Zhang *, Masataka Tanaka, Toshiro Matsumoto

Faculty of Engineering, Department of Mechanical Systems Engineering, Shinshu University, 4-17-1 Wakasato, Nagano 380-8553, Japan

Abstract

The unique thermal properties of carbon nanotubes (CNT) may offer possibilities for the development of fundamentally new composite materials. Numerical simulation for such CNT-based composites usually demands extremely large and expensive computer resources. In preliminary computations, temperature distribution in the CNT has been turned out to be almost uniform, due to its exceptionally high heat conductivity in comparison with the host polymer. This feature allows us to considerably simplify the mathematical model of the heat conduction in CNT composites. In the proposed approach, the host polymer is the only domain which is modeled, while the CNTs are treated as heat superconductors with constant and unknown temperatures constrained at their surfaces. As a result, the computational scale is reduced substantially. The hybrid boundary node method is applied in this study. Numerical examples clearly demonstrate the efficiency and sufficient accuracy of the proposed approach.
© 2004 Published by Elsevier B.V.

Keywords: Nano-composite; Heat conductivity; Hybrid boundary node method; Simplified approach

1. Introduction

Carbon nanotubes (CNT) have been attracting considerable attentions from both scientists and engineers for their remarkable mechanical and electronic properties over the last decade. Intensive researches have been carried out on these quasi-one-dimensional structures for their production, physical properties and possible applications [1,2]. Composed of the same atoms, CNTs are related to both graphite and diamond which are known for their high thermal conductivities. Thus, CNTs and CNT-based

---

* Corresponding author. Tel.: +81 26 269 5123.
E-mail address: zhangjm@homer.shinshu-u.ac.jp (J. Zhang).

composites potentially possess excellent heat conducting properties, and may be attractive for heat transport management in miniature device components.

A few experiments have been conducted to measure the thermal conductivities of mats of compressed ropes of CNTs [3,4], in which values of thermal conductivity ranging from 1750 to 5850 W/m K were reported. The direct measurements of the heat conductivity of individual CNT were also tried recently, and a value of 3000 W/m K was observed at room temperature [5]. Several preliminary numerical experiments based on molecular dynamics (MD) simulations [6–8] has also been performed and even higher values, 6600 W/m K at 300 K, of the thermal conductivities have been obtained. Although the estimated values were different in each simulation, it is generally accepted that the CNTs possess excellent heat conductivity, comparable or even better than diamond. Very recently, the single wall carbon nanotubes (SWNTs) were used to enhance the thermal properties of industrial epoxy. In the work of Biercuk et al. [9], samples loaded with 1 wt% SWNTs were observed to show a 70% increase in heat conductivity at 40 K, and 125% at room temperature.

Numerical simulations may help us understand designs of such nanocomposites, however, in comparison with those for pure CNTs, little simulation work has been done so far for the thermal properties of the CNT-based composites. This is because MD simulations are limited to very small length and time scales and cannot deal with the larger models, due to the limitations in current computing power.

The concept of representative volume element (RVE) has been widely used for conventional fiber-reinforced composites at the microscale analyses [10]. Recently, Liu et al. [11,12] applied it for the study of the CNT-based composites for evaluating their mechanical properties. In their study, a single nanotube with a surrounding matrix material was modeled as an RVE, with properly applied boundary and interface conditions to account for the effects of the surrounding materials. Then, elastic behavior of the RVE was evaluated using the finite element method. In the same way, Fisher et al. [13] analyzed the effects of the CNT waviness on the equivalent Young's modulus of the composites using an RVE containing a curved CNT by the finite element method.

The aim of this study is to investigate the thermal properties of RVEs of CNT-based composites through numerical simulations based on 3-D potential theory. For the analysis of an RVE in which not only single but also many CNTs are randomly distributed, there are two major difficulties in the standard numerical methods like FEM or BEM. One is that both may face severe difficulties in discretization of the domain geometry in question. This is more serious especially in FEM models where meshing of the solid geometries within CNT-reinforced polymers may be extremely complicated. The other is that the computational scale becomes extremely large and exceeds the current computing power. Because of the very thin and slender structure of the CNTs, a large number of nodes or elements are required to discretize them so that the steep gradients of the physical quantities close to the interface between the CNT and the matrix are captured accurately in the simulations. Moreover, at each node on the interface between the CNT and the matrix, both the temperature and the normal heat flux are unknown, so that the total degrees of freedom in the overall system of equations considerably increase.

To alleviate the first difficulty, the hybrid boundary node method (Hybrid BNM) can be used [14–18]. By combining a modified functional with the moving least squares (MLS) approximation, the Hybrid BNM becomes a truly meshless boundary-only method. The Hybrid BNM requires only discrete nodes located on the surface of the domain and its parametric representation. As the parametric representation of created geometry is used in all CAD software packages it should be possible to exploit their *Open Architecture* features and handle truly arbitrary geometry.

In preliminary computations [19], a distinct feature of temperature distribution was revealed. The temperatures within the entire CNT were turned out to be almost uniform. The main reason for this phenomenon is that almost the entire heat flux flows through the CNT, due to its high heat conductivity, higher than that of the matrix by several orders of magnitude. In light of this observation, a simplified approach is proposed in this paper. In the proposed approach, the CNTs are treated as heat superconduc-

tors and uniform temperature distribution within the entire body of each CNT is assumed. As a result, the total degrees of freedom are reduced substantially.

In this paper, the Hybrid BNM is first incorporated into a multi-domain solver in Section 2. Then, formulations for the simplified approach are derived in Section 3. Numerical examples verifying the validity and demonstrating the efficiency of the simplified approach are presented in Section 4. The paper ends with conclusions in Section 5.

2. Hybrid BNM formulations for the multi-domain solver

Suppose that n CNTs are distributed in a polymer matrix which makes an RVE. It is assumed that both the CNTs and the matrix are continua of linear, isotropic and homogenous materials with given heat conductivities. A steady state heat conduction problem governed by Laplace's equation with proper boundary conditions is considered for each CNT and the matrix domains.

The hybrid boundary node method is based on a modified variational principle, in which there are three independent variables, namely:

- temperature within the domain, ϕ;
- boundary temperature, $\tilde{\phi}$;
- boundary normal heat flux, $\widetilde{q}$.

Suppose further that N nodes are randomly distributed on the bounding surface of a single domain. The temperature within the domain is approximated using the fundamental solutions as follows:

$$\phi = \sum_{I=1}^{N} \phi_I^s x_I,\tag{1}$$

and hence at a boundary point, the normal heat flux is given by

$$q = -\kappa \sum_{I=1}^{N} \frac{\partial \phi_I^s}{\partial n} x_I,\tag{2}$$

where ϕ_I^s is the fundamental solution with the source at a node $\mathbf{s}_I$, κ is the heat conductivity and x_I are the unknown parameters. For 3-D steady state heat conduction problems, the fundamental solution can be written as

$$\phi_I^s = \frac{1}{\kappa} \frac{1}{4\pi r(Q, \mathbf{s}_I)},\tag{3}$$

where Q is a field point; $r(Q, \mathbf{s}_I)$ is the distance between the point Q and the node $\mathbf{s}_I$.

The boundary temperature and the normal heat flux are interpolated by moving least square (MLS) approximation

$$\tilde{\phi}(\mathbf{s}) = \sum_{I=1}^{N} \Phi_I(\mathbf{s})\hat{\phi}_I,\tag{4}$$

and

$$\widetilde{q}(\mathbf{s}) = \sum_{I=1}^{N} \Phi_I(\mathbf{s})\hat{q}_I.\tag{5}$$

In the foregoing equations, $\Phi_I(\mathbf{s})$ is the shape function of MLS approximation; $\hat{\phi}_I$ and $\hat{q}_I$ are the nodal values of temperature and normal flux, respectively.

For the polymer domain, the following set of Hybrid BNM equations can be written

$$\begin{bmatrix} U^{\mathrm{p}}_{00} & U^{\mathrm{p}}_{01} & \cdots & U^{\mathrm{p}}_{0n} \\ U^{\mathrm{p}}_{10} & U^{\mathrm{p}}_{11} & \cdots & U^{\mathrm{p}}_{1n} \\ \vdots & \vdots & \ddots & \vdots \\ U^{\mathrm{p}}_{n0} & U^{\mathrm{p}}_{n1} & \cdots & U^{\mathrm{p}}_{nn} \end{bmatrix} \begin{Bmatrix} x^{\mathrm{p}}_0 \\ x^{\mathrm{p}}_1 \\ \vdots \\ x^{\mathrm{p}}_n \end{Bmatrix} = \begin{Bmatrix} H^{\mathrm{p}}_0 \hat{\phi}^{\mathrm{p}}_0 \\ H^{\mathrm{p}}_0 \hat{\phi}^{\mathrm{p}}_1 \\ \vdots \\ H^{\mathrm{p}}_n \hat{\phi}^{\mathrm{p}}_n \end{Bmatrix}, \tag{6}$$

$$\begin{bmatrix} V^{\mathrm{p}}_{00} & V^{\mathrm{p}}_{01} & \cdots & V^{\mathrm{p}}_{0n} \\ V^{\mathrm{p}}_{10} & V^{\mathrm{p}}_{11} & \cdots & V^{\mathrm{p}}_{1n} \\ \vdots & \vdots & \ddots & \vdots \\ V^{\mathrm{p}}_{n0} & V^{\mathrm{p}}_{n1} & \cdots & V^{\mathrm{p}}_{nn} \end{bmatrix} \begin{Bmatrix} x^{\mathrm{p}}_0 \\ x^{\mathrm{p}}_1 \\ \vdots \\ x^{\mathrm{p}}_n \end{Bmatrix} = \begin{Bmatrix} H^{\mathrm{p}}_0 \hat{q}^{\mathrm{p}}_0 \\ H^{\mathrm{p}}_1 \hat{q}^{\mathrm{p}}_1 \\ \vdots \\ H^{\mathrm{p}}_n \hat{q}^{\mathrm{p}}_n \end{Bmatrix}, \tag{7}$$

where superscripts p, subscripts 0 and $k, k = 1, \ldots, n$ stand for polymer, quantities exclusively associated with a domain, and quantities associated with the interface between the k-th nanotube and the matrix, respectively. The sub-matrices $[U]$, $[V]$ and $[H]$ are given as

$$U_{IJ} = \int_{\Gamma^J_s} \phi^s_I v_J(Q) \, \mathrm{d}\Gamma, \tag{8}$$

$$V_{IJ} = \int_{\Gamma^J_s} q^s_I v_J(Q) \, \mathrm{d}\Gamma, \tag{9}$$

$$H_{IJ} = \int_{\Gamma^J_s} \Phi_I(\mathbf{s}) v_J(Q) \, \mathrm{d}\Gamma, \tag{10}$$

where Γ^J_s is a regularly shaped local region around a given node $\mathbf{s}_J$, v_J is a weight function and $\mathbf{s}$ is a field point on the boundary. (For full details of Hybrid BNM refer to [18]).

Similarly, for the k-th nanotube domain we have

$$\begin{bmatrix} U^{t_k}_{00} & U^{t_k}_{0i} \\ U^{t_k}_{i0} & U^{t_k}_{ii} \end{bmatrix} \begin{Bmatrix} x^{t_k}_0 \\ x^{t_k}_i \end{Bmatrix} = \begin{Bmatrix} H^{t_k}_0 \hat{\phi}^{t_k}_0 \\ H^{t_k}_i \hat{\phi}^{t_k}_i \end{Bmatrix}, \tag{11}$$

$$\begin{bmatrix} V^{t_k}_{00} & V^{t_k}_{0i} \\ V^{t_k}_{i0} & V^{t_k}_{ii} \end{bmatrix} \begin{Bmatrix} x^{t_k}_0 \\ x^{t_k}_i \end{Bmatrix} = \begin{Bmatrix} H^{t_k}_0 \hat{q}^{t_k}_0 \\ H^{t_k}_i \hat{q}^{t_k}_i \end{Bmatrix}, \tag{12}$$

where the superscript t_k stands for the k-th nanotube and the subscript i indicates the quantities associated with the interface between the k-th nanotube and the matrix.

At the interface between a nanotube and the polymer both the temperature and heat fluxes must be continuous, i.e.,

$$\{\phi^{\mathrm{p}}_k\} = \{\phi^{t_k}_i\}, \tag{13}$$

and

$$\{q^{\mathrm{p}}_k\} = -\{q^{t_k}_i\}. \tag{14}$$

Using the continuity conditions, Eqs. (6), (7), (11) and (12) can be assembled into the following expression:

$$
\begin{bmatrix}
A_{00}^{p} & A_{01}^{p} & \mathbf{0} & \mathbf{0} & \cdots & A_{0k}^{p} & \mathbf{0} & \mathbf{0} \\
U_{10}^{p} & U_{11}^{p} & -U_{ii}^{t_1} & -U_{i0}^{t_1} & \cdots & U_{1k}^{p} & \mathbf{0} & \mathbf{0} \\
V_{10}^{p} & V_{11}^{p} & V_{ii}^{t_1} & V_{i0}^{t_1} & \cdots & V_{1k}^{p} & \mathbf{0} & \mathbf{0} \\
\mathbf{0} & \mathbf{0} & A_{0i}^{t_1} & A_{00}^{t_1} & \cdots & \mathbf{0} & \mathbf{0} & \mathbf{0} \\
\vdots & \vdots & \vdots & \vdots & \ddots & \vdots & \vdots & \vdots \\
U_{n0}^{p} & U_{n1}^{p} & \mathbf{0} & \mathbf{0} & \cdots & U_{nn}^{p} & -U_{ii}^{t_n} & -U_{i0}^{t_n} \\
V_{n0}^{p} & V_{n1}^{p} & \mathbf{0} & \mathbf{0} & \cdots & V_{nn}^{p} & V_{ii}^{t_n} & V_{i0}^{t_n} \\
\mathbf{0} & \mathbf{0} & \mathbf{0} & \mathbf{0} & \cdots & \mathbf{0} & A_{0i}^{t_n} & A_{00}^{t_n}
\end{bmatrix}
\begin{Bmatrix}
x_0^{p} \\ x_1^{p} \\ x_i^{t_1} \\ x_0^{t_1} \\ \vdots \\ x_n^{p} \\ x_i^{t_n} \\ x_0^{t_n}
\end{Bmatrix}
=
\begin{Bmatrix}
H_0^{p} d_0^{p} \\ \mathbf{0} \\ \mathbf{0} \\ H_0^{t_1} d_0^{t_1} \\ \vdots \\ \mathbf{0} \\ \mathbf{0} \\ H_0^{t_n} d_0^{t_n}
\end{Bmatrix},
\tag{15}
$$

where $[A_{00}^{p}]$, $[A_{01}^{p}]$ and $\{d_0^{p}\}$ are formed by merging $[U_{00}^{p}]$ and $[V_{00}^{p}]$, $[U_{01}^{p}]$ and $[V_{01}^{p}]$, and $\{\hat{\phi}_0^{p}\}$ and $\{\hat{q}_0^{p}\}$ respectively, according to the known boundary conditions. For degrees of freedom with prescribed temperature, the related elements in $\{\hat{\phi}_0^{p}\}$ are selected for $\{d_0^{p}\}$, and the corresponding rows of $[U_{00}^{p}]$ and $[U_{01}^{p}]$ are selected for $[A_{00}^{p}]$ and $[A_{01}^{p}]$; otherwise, elements in $\{\hat{q}_0^{p}\}$ are selected for $\{d_0^{p}\}$ and the corresponding rows in $[V_{00}^{p}]$ and $[V_{01}^{p}]$ are selected for $[A_{00}^{p}]$ and $[A_{01}^{p}]$. In the same way, $[A_{00}^{t_k}]$, $[A_{0i}^{t_k}]$ and $\{d_0^{t_k}\}$, are formed by merging $[U_{00}^{t_k}]$ and $[V_{00}^{t_k}]$, $[U_{0i}^{t_k}]$ and $[V_{0i}^{t_k}]$, and $\{\hat{\phi}_0^{t_k}\}$ and $\{\hat{q}_0^{t_k}\}$, respectively.

The set of Eq. (15) is solved for the unknown parameters x by the standard Gauss elimination solver, and then, by back-substitution into Eqs. (6), (7), (11) and (12), the boundary unknowns are obtained either on the interfaces or the external boundary surfaces. As demonstrated, the multi-domain Hybrid BNM is a boundary-only meshless approach. No boundary elements are used for either interpolation or integration purposes. Therefore, it may alleviate the discretization difficulty to a large extent for complicated geometries.

3. Formulations for the simplified approach

As mentioned in the introduction, the unusually high heat conductivity of the CNTs in comparison with the polymer makes the temperature distribution within an individual CNT almost uniform. This feature may allow us to simplify the modeling of the CNT-based composites. In this section the formulations for the simplified approach are developed, where only single domain, namely the polymer matrix is modelled. Each CNT is treated as a heat superconductor with only one constant temperature constrained at its surface.

Using the hybrid boundary node method, the same Eqs. (6) and (7) in Section 2 for the polymer domain can be obtained. By combining Eqs. (6) and (7), we have the following equation:

$$
\begin{bmatrix}
A_{00} & A_{01} & \cdots & A_{0n} \\
U_{10} & U_{11} & \cdots & U_{1n} \\
\vdots & \vdots & \ddots & \vdots \\
U_{n0} & U_{n1} & \cdots & U_{nn}
\end{bmatrix}
\begin{Bmatrix}
x_0 \\ x_1 \\ \vdots \\ x_n
\end{Bmatrix}
=
\begin{Bmatrix}
H_0 d_0 \\ H_0 \hat{\phi}_1 \\ \vdots \\ H_0^{p} \hat{\phi}_n
\end{Bmatrix},
\tag{16}
$$

where the superscript p is omitted for clarity as there is only single domain considered here, and $[A_{0k}]$, $k = 0, 1, \ldots, n$ and $\{d_0\}$ are formed by merging $[U_{0k}]$ and $[V_{0k}]$ and $\{\hat{\phi}_0\}$ and $\{\hat{q}_0\}$, respectively, in the same way as explained in Section 2.

Suppose that m_k nodes are located at the interface of the k-th nanotube with the polymer, and a constant temperature ϕ_c^k is prescribed, namely

$$\{\hat{\boldsymbol{\phi}}_k\} = \{\mathbf{1}\}_k \phi_c^k, \tag{17}$$

where $\{\boldsymbol{\phi}_k\}$ is the nodal values of temperature at the interface; $\{\mathbf{1}\}_k$ is a column vector of m_k dimensions with all the elements equals 1. By substituting Eq. (17) into Eq. (16) for all the interfaces, the following equation is obtained,

$$\begin{bmatrix} \boldsymbol{A}_{00} & \boldsymbol{A}_{01} & \cdots & \boldsymbol{A}_{0n} & \mathbf{0} & \cdots & \mathbf{0} \\ \boldsymbol{U}_{10} & \boldsymbol{U}_{11} & \cdots & \boldsymbol{U}_{1n} & \boldsymbol{H}_1\{\mathbf{1}\}_1 & \cdots & \mathbf{0} \\ \vdots & \vdots & \ddots & \vdots & \vdots & \ddots & \vdots \\ \boldsymbol{U}_{n0} & \boldsymbol{U}_{n1} & \cdots & \boldsymbol{U}_{nn} & \mathbf{0} & \cdots & \boldsymbol{H}_n\{\mathbf{1}\}_n \end{bmatrix} \begin{Bmatrix} \boldsymbol{x}_0 \\ \boldsymbol{x}_1 \\ \vdots \\ \boldsymbol{x}_n \\ \phi_c^1 \\ \vdots \\ \phi_c^n \end{Bmatrix} = \begin{Bmatrix} \boldsymbol{H}_0\boldsymbol{d}_0 \\ \mathbf{0} \\ \vdots \\ \mathbf{0} \end{Bmatrix}. \tag{18}$$

In the above set of equations, there are n (the number of CNTs) more unknowns than the number of equations, because we have introduced one more unknown, i.e. the constant temperature, for each CNT. In order to solve Eq. (18), we need to add n additional equations. These equations can be obtained by using energy conservation law. Actually, for a steady state heat conduction, the rate of thermal energy flowing into a CNT must equal to the rate of energy flowing out. Therefore, the following heat flux relationship exists at the surface of the k-th CNT,

$$\int_{C_k} q \, \mathrm{d}\Gamma = 0, \tag{19}$$

where C_k represents the outer surface of the k-th CNT. Substituting Eq. (2) into (19) and omitting the common factor κ, we have

$$\sum_{I=1}^{N} \int_{C_k} \frac{\partial \phi_I^s}{\partial n} \, \mathrm{d}\Gamma x_I = 0. \tag{20}$$

In Eq. (20) C_k is a closed surface and ϕ_I^s is the fundamental solution with the source point located at the node $\mathbf{s}_I$, hence the following integral identity [20] holds,

$$\int_{C_k} \frac{\partial \phi_I^s}{\partial n} \, \mathrm{d}\Gamma = \begin{cases} 1 & \forall \mathbf{s}_I \in C_k, \\ 0 & \forall \mathbf{s}_I \in C_k. \end{cases} \tag{21}$$

Therefore, the coefficients in equation (20) are either 1 or 0. For nodes located on the surface of the k-th CNT, they are 1, otherwise they are 0. Appending Eq. (20) to Eq. (18) for all CNTs, we obtain the final set of algebraic equations which can uniquely determine the unknown parameter $\boldsymbol{x}$.

$$
\begin{bmatrix}
A_{00}^0 & A_{01}^0 & \cdots & A_{0n}^0 & \mathbf{0} & \cdots & \mathbf{0} \\
U_{10}^0 & U_{11}^0 & \cdots & U_{1n}^0 & H_1\{1\}_1 & \cdots & \mathbf{0} \\
\mathbf{0} & \{1\}_1^{\mathrm{T}} & \cdots & \mathbf{0} & 0 & \cdots & 0 \\
\vdots & \vdots & \ddots & \vdots & \vdots & \ddots & \vdots \\
U_{n0}^0 & U_{n1}^0 & \cdots & \mathbf{U}_{nn}^0 & \mathbf{0} & \cdots & H_n\{1\}_n \\
\mathbf{0} & \mathbf{0} & \cdots & \{1\}_n^{\mathrm{T}} & 0 & \cdots & 0
\end{bmatrix}
\begin{Bmatrix}
x_0 \\ x_1 \\ \vdots \\ x_n \\ \phi_c^1 \\ \vdots \\ \phi_c^n
\end{Bmatrix}
=
\begin{Bmatrix}
H_0 d_0 \\ \mathbf{0} \\ 0 \\ \vdots \\ \mathbf{0} \\ 0
\end{Bmatrix}.
\tag{22}
$$

Comparing Eq. (22) with Eq. (15), it can be seen that the total number of degrees of freedom in the simplified modeling is reduced considerably. For each CNT, only one algebraic equation is added. Furthermore, the coefficients of these algebraic equations are either 1 or 0. Calculations of them are avoided. Therefore, both the CPU time and memory usage can be saved significantly.

4. Numerical results

4.1. An RVE containing single CNT

An RVE model with single CNT embedded is first investigated. The geometry and boundary conditions are presented in Fig. 1(a)–(c). Fig. 1(c) shows the computational model discretized with boundary nodes.

The dimensions of the RVE are: for the matrix, length $L = 100$ nm, $H = 20$ nm; for the CNT, length $L_c = 50$, outer radius $R = 5$ nm, thickness $D = 0.4$ nm (which is close to the theoretical value of 0.34 nm for SWCNT thickness). The heat conductivities used for the CNT and matrix (Polycarbonate) are:
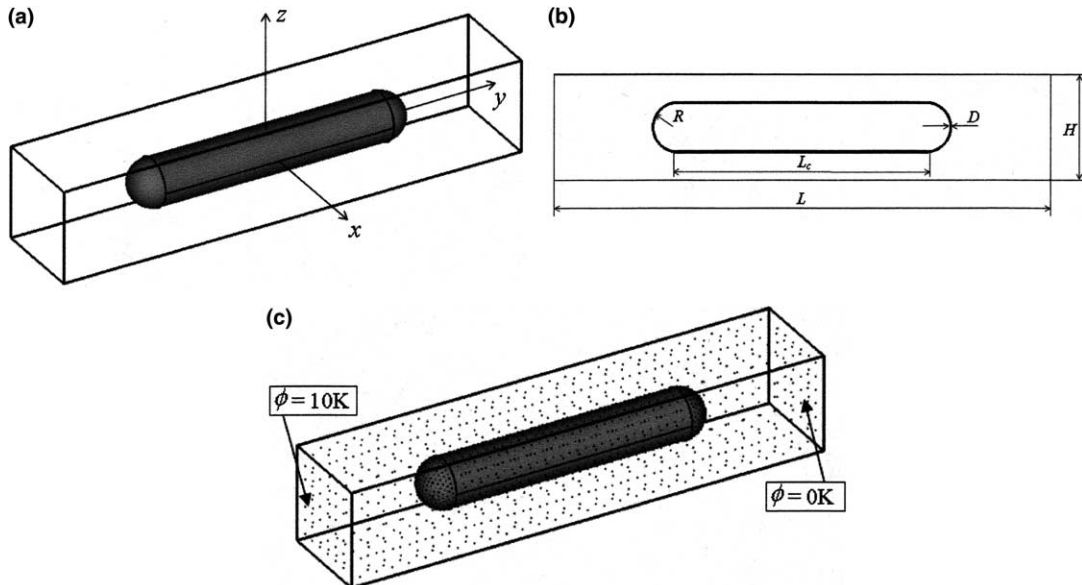
Fig. 1. Nanoscale representative volume element with single nanotube embedded. (a) The unit model and coordinates system. (b) Dimensions of the unit model. (c) Discretization with boundary nodes.

CNT: $\kappa^{t} = 1750$ W/m K;

Matrix: $\kappa^{m} = 0.37$ W/m K.

These values of the dimensions and material constants are within the wide ranges of those for CNTs reported in literature [1–9].

Homogeneous boundary conditions are considered here, namely uniform temperatures of 10 and 0 K imposed at the two end faces of the RVE, respectively, and heat flux free at the other four side faces (see Fig. 1(c)). This boundary condition set allows us to estimate equivalent heat conductivity of CNT-based composite in the axial direction. Assuming homogeneous material properties and using Fourier's law, the formula for equivalent heat conductivity can be written as

$$\kappa = -\frac{qL}{\Delta\phi}, \tag{23}$$

where κ represents the heat conductivity; q is the heat flux density, L the length of the RVE in the axial direction and $\Delta\phi$ the temperature difference between the two end faces.

The problem was solved using both the multi-domain solver described in Section 2 and the simplified approach outlined in Section 3. When solved by the multi-domain solver, the whole CNT was modeled as one domain and the polymer as the other. The inner face of the CNT was prescribed as flux free, while the outer face was handled as the interface between the two domains. Continuity conditions, i.e. Eqs. (13) and (14) were applied at the interface. When solved by the simplified approach, only single domain, namely the polymer, was modeled, while, instead of modeling the CNT as a domain, an unknown uniform temperature was constrained at the interface.

Numerical results for the temperature along two horizontal lines (one line is from $(0, -49, -5.1)$ to $(0, 49, -5.1)$, the other from $(0, -49, -9)$ to $(0, 49, -9)$) are presented in Fig. 2. In this figure and thereafter, MS and SA stand for multi-domain solver and simplified approach, respectively. It is seen that results obtained by the two methods agree excellently with each other. Fig. 3 shows numerical results for the heat flux in the axial direction along three vertical lines (the first line is from $(0, 30.1, -9.5)$ to $(0, 30.1, 9.5)$, the second line from $(0, 35, -9.5)$ to $(0, 35, 9.5)$, and the third from $(0, 49.5, -9.5)$ to $(0, 49.5, 9.5)$). Again, they are in good
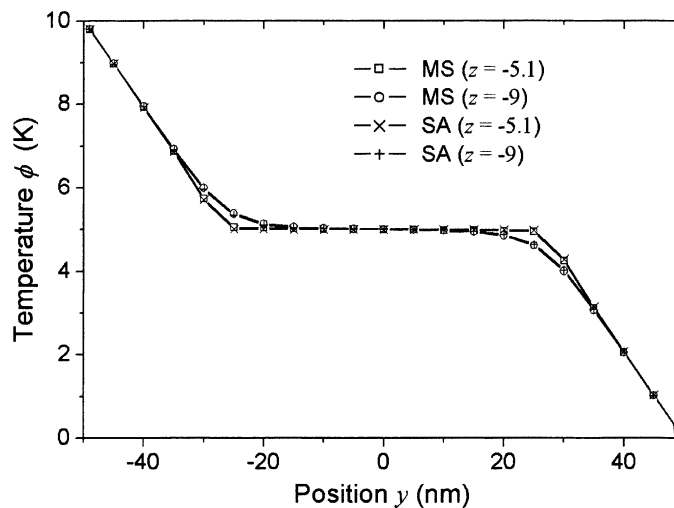
Fig. 2. Temperature distribution along the axial lines. MS: multi-domain solver, SA: simplified approach.
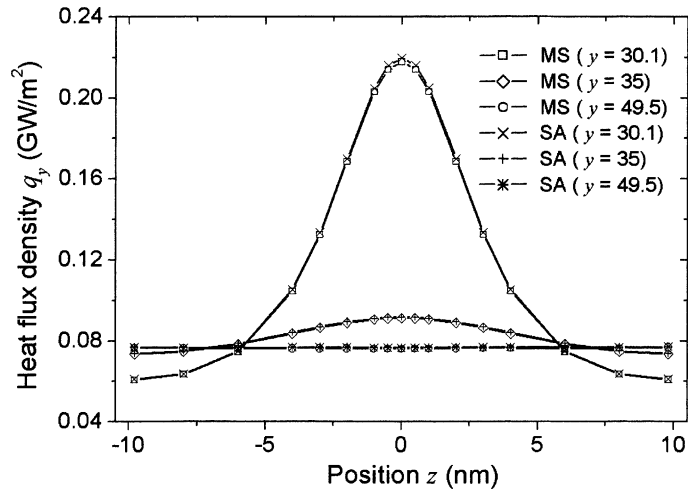
Fig. 3. Heat flux distribution along the vertical lines. MS: multi-domain solver, SA: simplified approach.

agreement. In Fig. 2, an obvious feature of the temperature distribution is observed that the temperature in the matrix first decreases from the prescribed temperature value at the square end face, then remains almost constant at the segments near the CNT, and finally continues to decrease to the lowest temperature at the other square end face. This observation is consistent with the physical interpretation. Due to that the heat conductivity of the CNT is several orders of magnitude higher than that of the host polymer, almost the entire flux flows through the CNT. Therefore, nearly no flux flows in the matrix in the segments near the CNT, and the temperature at these locations is almost uniform. The corresponding heat flux concentrations can be easily seen near the tips of the CNT in Fig. 3.

Preliminary computations [19] have also shown that the equivalent heat conductivity of the RVE is mainly determined by the lengths of the RVE and the CNT, and relatively less affected by the height of the RVE (H in Fig. 1(b)). This is because the heat conduction problem considered here is in one dimension only, namely, in the axial direction of the CNT. The accuracy of the simplified modeling does not depend on the actual geometrical dimensions of RVE. It is affected only by the ratio of the heat conductivities of the host polymer and CNT.

To compare the efficiency of the two methods, the total number of degrees of freedom in the overall system of equation, and the times spent for computing the matrices and for solving the overall equation are listed in Table 1. Numerical results of equivalent heat conductivity from both the methods are also compared in Table 1. The difference between the results of equivalent heat conductivity is only 0.67%, while both the memory usage and CPU time are reduced substantially in the simplified approach.

Table 1
CPU timing results for both methods

	Total degrees of freedom	CPU seconds for integration	CPU seconds for solving equation	Equivalent heat conductivity
Multi-domain solver	4402	294	477	0.7719
Simplified approach	2193	144	62	0.7771

4.2. An RVE containing two CNTs

In order to further justify the simplified approach, an RVE containing two CNTs is considered in this section. Dimensions and the boundary conditions for the outer faces of the RVE are remained the same as the single CNT model. Two CNTs of conformable size are coaxially aligned within the RVE depicted in Fig. 4. Sizes of the CNT of Section 4.1 are kept for each CNT, except for lengths, which are given in Fig. 4. The value of heat conductivity for the polymer used in this model is the same as the previous single CNT model. In order to achieve better agreements between the two methods, a higher value, namely 6000 W/m K is selected for the CNTs, which is still within the range of those for CNTs reported in Ref. [6]. Like the single CNT model, this model was also solved by both the multi-domain solver and the simplified approach, respectively. Since the CNTs are treated as heat superconductors in the simplified modeling, thus we can expect better agreements of results between the simplified approach and the multi-domain solver if a higher value of heat conductivity is used for the CNTs in the multi-domain modeling. Results of temperatures along two horizontal lines (one is from $(0, -49, -5.1)$ to $(0, 49, -5.1)$, the other from $(0, -49, -9)$ to $(0, 49, -9)$) are shown in Fig. 5. Fig. 6 presents the heat fluxes in the axial direction along four vertical lines (the first line is from $(0, 0, -9.5)$ to $(0, 0, 9.5)$, the second line from $(0, 4.9, -9.5)$ to $(0, 4.9, 9.5)$, the third from $(0, 40.1, -9.5)$ to $(0, 40.1, 9.5)$, and the fourth from $(0, 45, -9.5)$ to $(0, 45, 9.5)$). Again, it is seen that numerical results for both the temperature and flux obtained by the simplified approach are excellent approximations of that by the multi-domain solver. Comparing Fig. 6 with Fig. 3, it is seen that better agreement of flux concentration at the locations close to the tip points of the CNTs is achieved than the single CNT model. This is what we have expected.
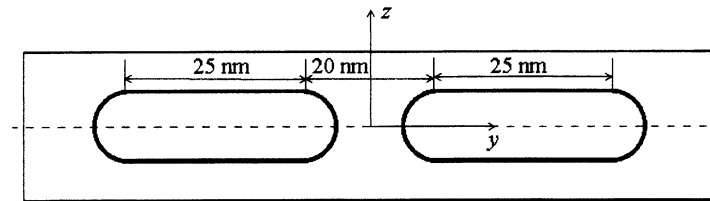
Fig. 4. Nanoscale representative volume element with two CNTs embedded.
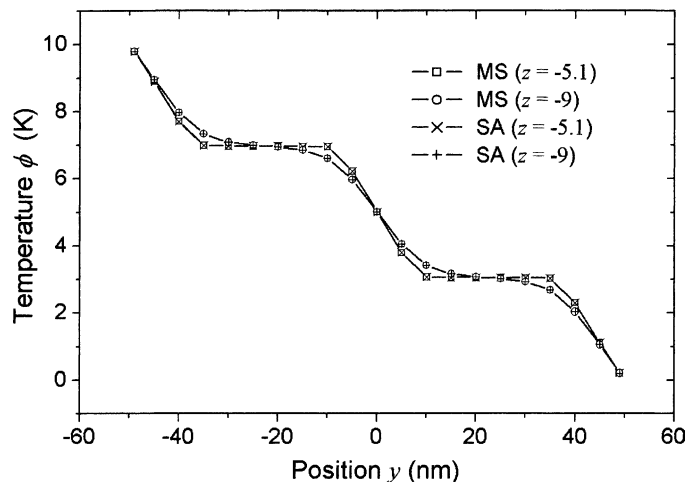
Fig. 5. Temperature distribution along the axial lines. MS: multi-domain solver, SA: simplified approach.
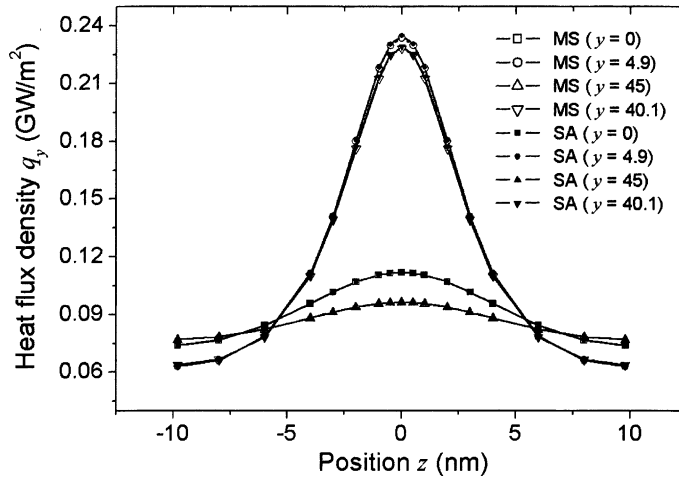
Fig. 6. Heat flux distribution along the vertical lines. MS: multi-domain solver, SA: simplified approach.

4.3. Maximum temperature difference within a CNT

One of the key factors that result in the uniform temperature within a CNT is the significant difference of heat conductivity between the CNTs and the polymer. In order to study the influence of the difference of heat conductivity on the temperature distribution within the RVE, the maximum temperature difference within the CNT has been calculated as a function of the ratio of the heat conductivity between the CNT and the polymer matrix $C_r = \kappa^{CNT}/\kappa^{matrix}$. The dimensions and parameters of Section 4.1 are the kept, except for C_r, which varies from 1 to 10 000. For each value of C_r, the conductivity of the polymer is held constant at 0.37 W/m K. In the computations, the multi-domain solver is employed. The maximum temperature difference, $\Delta\phi_{max}$, within the CNT is represented by that between the two end tip points (0, 30, 0) and (0, −30, 0). Results are presented in Fig. 7. As expected, $\Delta\phi_{max}$ decreases with C_r increasing. When C_r grows up to 2000, $\Delta\phi_{max}$ is only 2.5% that in the case of homogeneity ($C_r = 1.0$). Since the lowest value
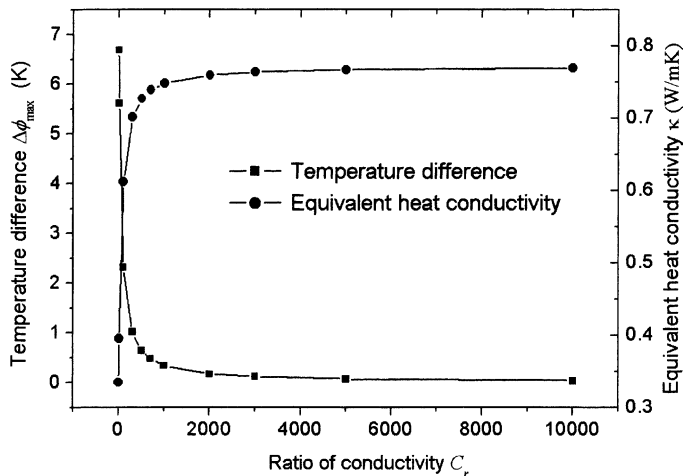
Fig. 7. Equivalent heat conductivity of the RVE for various ratios C_r.

of ratio of heat conductivity between the CNTs and a polymer, ever reported in literature, is much higher than 2000, the CNTs can be treated as a heat superconductor without loss in accuracy. The effective heat conductivities estimated by Eq. (23) for various C_r are also presented in Fig. 7. It can be seen that the equivalent heat conductivity converges to a specific value when the ratio grows larger. When the ratio is bigger than 2000, the exact value of heat conductivity of the CNT has little effect on the equivalent heat conductivity of the RVE.

5. Conclusions

In a CNT-based composite, the CNT phase possesses exceptionally high heat conductivity, while the heat conductivity of the host polymer phase is relatively very low. The significant difference of heat conductivity makes the simulation of thermal behavior of the composites rather challenging. On the other hand, it also provides the opportunities to simplify the modeling. In this paper, a simplified approach is proposed, in which each CNT is treated as a heat superconductor and a constant temperature within the entire body of the CNT is assumed. Formulations for both full modeling (the multi-domain solver) and the simplified approach are presented.

The simplified approach was validated by studying the examples of an RVE with single and two CNT(s) embedded, solved using the multi-domain solver and the simplified approach, respectively. Numerical results obtained from both the approaches are presented and an excellent consistency demonstrated. The influence of heat conductivity ratio of CNT to the polymer matrix on the accuracy of the simplified approach was also investigated. All calculations clearly demonstrate that the heat conducting behavior of CNT-based composites can be simulated by the simplified approach without loss in accuracy.

The simplified approach provides remarkable improvements to overall computational efficiency and allows for the solution of complicated problems using less computer memory, thus increases the number of CNTs contained in an RVE that can be analyzed within the available computer resources. Combining the Hybrid BNM with the fast multi-pole techniques [21,22] to further reduce the memory requirements and computational time is underway.

References

[1] M. Endo, Y.A. Kim, K. Nishimura, T. Matushita, T. Hayashi, From vapor-grown carbon fibers (VGCFs) to carbon nanotubes, in: L.P. Biro, C.A. Bernardo, G.G. Tibbetts, Ph. Lambin (Eds.), Carbon filaments and Nanotubes: Common origins, Differing Applications, NATO Science Series E: Applied Sciences, vol. 372, Kluwer Academic Publishers, 2001, pp. 51–61.
[2] M. Endo, Y.A. Kim, T. Hayashi, K. Nishimura, T. Matushita, K. Miyashita, M.S. Dresselhaus, Vapor-grown carbon fibers (VGCFs): basic properties and their battery applications, Carbon 39 (2001) 1287–1297.
[3] J. Hone, M. Whitney, C. Piskoti, A. Zettl, Thermal conductivity of single-walled nanotubes, Phys. Rev. B 59 (4) (1999) 2514–2516.
[4] W. Yi, L. Lu, D.L. Zhang, Z.W. Pan, S.S. Xie, Linear specific heat of carbon nanotubes, Phys. Rev. B 59 (1999) 9015–9018.
[5] P. Kim, L. Shi, A. Majumdar, P1. McEuen, Thermal transport measurements of individual multiwalled nanotubes, Phys. Rev. Lett. 87 (2001), 215502-1.
[6] S. Berber, Y.-K. Kown, D. Tomanek, Unusually high thermal conductivity of carbon nanotubes, Phys. Rev. Lett. 84 (20) (2000) 4613–4617.

[7] M.A. Osman, D. Srivastava, Temperature dependence of the thermal conductivity of single-wall carbon nanotubes, Nanotechnology 12 (1) (2001) 24.

[8] J. Che, T. Cagin, W.A. Goddard III, Thermal conductivity of carbon nanotubes, Nanotechnology 11 (2000) 65–69.

[9] MJ. Biercuk, M.C. Llaguno, M. Radosavljevic, J.K. Hyun, A.T. Johnson, J.E. Fischer, Carbon nanotube composites for thermal management, Appl. Phys. Lett. 80 (15) (2002) 2767–2769.

[10] M.W. Hyer, Stress Analysis of Fiber-Reinforced Composite Materials, McGraw-Hill, Boston, 1998.

[11] Y.J. Liu, X.L. Chen, Evaluations of the effective material properties of carbon nanotube-based composites using a nanoscale representative volume element, Mech. Mater. 35 (2003) 69–81.

[12] X.L. Chen, Y.J. Liu, Square representative volume elements for evaluating the effective material properties of carbon nanotube-based composites, Comput. Mater. Sci. 29 (2004) 1–11.

[13] F.T. Fisher, R.D. Bradshaw, L.C. Brinson, Effects of nanotube waviness on the modulus of nanotube-reinforced polymers, Appl. Phys. Lett. 80 (24) (2002) 4647–4649.

[14] J.M. Zhang, Z.H. Yao, H. Li, A hybrid boundary node method, Int. J. Numer. Methods Engrg. 53 (2002) 751–763.

[15] J.M. Zhang, Z.H. Yao, Meshless regular hybrid boundary node method, Comput. Model. Engrg. Sci. 2 (2001) 307–318.

[16] J.M. Zhang, Z.H. Yao, M. Tanaka, The meshless regular hybrid boundary node method for 2-D linear elasticity, Engrg. Anal. Boundary Elements 27 (2003) 259–268.

[17] J.M. Zhang, Z.H. Yao, Analysis of 2-D thin structures by the meshless regular hybrid boundary node method, Acta Mech. Sinica 15 (2002) 36–44.

[18] J.M. Zhang, M. Tanaka, T. Matsumoto, Meshless analysis of potential problems in three dimensions with the hybrid boundary node method, Int. J. Numer. Methods Engrg. 59 (2004) 1147–1160.

[19] J.M. Zhang, M. Tanaka, T. Matsumoto, A. Guzik, Analysis of heat conduction in CNT-based composites using hybrid boundary node method, JSME International Journal Series A: Solid Mechanics and Material Engineering, vol. 47, in press.

[20] Y.J. Liu, T.J. Rudolphi, New identities for fundamental solutions and their applications to non-singular boundary element formulations, Comput. Mech. 24 (1999) 286–292.

[21] L. Greengard, V. Rokhlin, A new version of the fast multipole method for the Laplace equation in three dimensions, Acta Numerica (1997) 229–269.

[22] T. Nishida, K. Hayami, Application of the fast multipole method to the 3D BEM analysis of electron guns, in: M. Marchettia, C.A. Brebbia, M.H. Aliabadi (Eds.), Boundary Elements XIX, Computational Mechanics Publications, 1997, pp. 613–622.